Accepted refereed manuscript of:

Varley A, Tyler A, Dowdall M, Bondar Y & Zabrotski V (2017) An in situ method for the high resolution mapping of 137Cs and estimation of vertical depth penetration in a highly contaminated environment, *Science of the Total Environment*, 605-606, pp. 957-966.

DOI: 10.1016/j.scitotenv.2017.06.067

An *In situ* Method for the High Resolution Mapping of ^{137}Cs and Estimation of Vertical Depth Penetration in a Highly Contaminated Environment.

Adam Varley[β], Andrew Tyler[β], Mark Dowdall[α], Yuri Bondar,

[β] Department of. Biological and Environmental Sciences, University of Stirling, Stirling, FK9 4LA, United Kingdom

[α] Norwegian Radiation Protection Authority, Grini næringspark 13, 1332 Østerås, Norway

Abstract

The Chernobyl nuclear power plant meltdown has to date been the single largest release of radioactivity into the environment. As a result, radioactive contamination that poses a significant threat to human health still persists across much of Europe with the highest concentrations associated with Belarus, Ukraine and western Russia. Of the radionuclides still prevalent with these territories ^{137}Cs presents one of the most problematic remediation challenges. Principally, this is due to the localised spatial and vertical heterogeneity of contamination within the soil (~10's of meters), thus making it difficult to accurately characterise through conventional measurement techniques such as static *in situ* gamma-ray spectrometry or soil cores. Here, a practical solution has been explored, which utilises a large number of short-count time spectral measurements made using relatively inexpensive, lightweight, scintillators (sodium iodide and lanthanum bromide). This approach offers the added advantage of being able to estimate activity and burial depth of ^{137}Cs contamination in much higher spatial resolution compared to traditional approaches. During the course of this work, detectors were calibrated using the Monte Carlo simulations and depth distribution was estimated using the peak-to-valley ratio. Activity and depth estimates were then compared to five reference sites characterised using soil cores. Estimates were in good agreement with the reference sites, differences of ~25 % and ~50 % in total inventory were found for the three higher and two lower activity sites, respectively. It was concluded that slightly longer count times would be required for the lower activity (<1 MBq m^{-2}) sites. Modelling and reference site results suggest little advantage would be gained through the use of the substantially more expensive lanthanum bromide detector over the sodium iodide detector. Finally, the potential of the approach was demonstrated by mapping one of the sites and its surrounding area in high spatial resolution.

Keywords

Cs-137, *in situ*, field gamma-ray spectrometry, peak-to-valley, PVT, Chernobyl

Highlights

- Chernobyl-derived ^{137}Cs poses a risk to human health.
- Highly heterogeneous contamination within tens of kilometres of Chernobyl particularly difficult to characterise.
- Numerous short count time gamma-ray measurements can address spatial resolution issues.
- Peak-to-valley method provides improved depth and activity estimates.

1. Introduction

The accident that occurred at the Chernobyl Nuclear Power Plant (ChNPP) in April 1986 resulted in the radioactive contamination of wide areas of Europe and, to a greater extent, the territories of Belarus, Ukraine and the western Russian Federation. In areas of south Belarus the deposition exceeded 1500 kBq/m^2 ^{137}Cs, 3 orders of magnitude greater than that which resulted from atmospheric nuclear weapons as of 1986 (UNSCEAR, 2000). As a result of the accident, a total area exceeding 60,000 km^2 of forested land was contaminated, including over 20,000 km^2 of the Gomel and Mogilev regions of Belarus in addition to areas near Kiev and in the Russian Federations' Bryansk region. The primary contaminants as a result of the accident were ^{137}Cs, ^{90}Sr and ^{239}Pu. Highest levels of contamination, in excess of 1.4 MBq/m^2 of ^{137}Cs occur with the southernmost parts of the reserves territory over lands nearest the Chernobyl reactor while localised areas of high contamination can be found distributed throughout the reserve. Sr-90 is present at densities up to 3 MBq/m^2 while ^{241}Am levels have approximately doubled over the past twenty years and now approach 0.1 MBq/m^2 in places as a result of ingrowth from ^{241}Pu (Smith and Beresford, 2002). Actinides such as ^{238}Pu and ^{239,240}Pu are present at levels up to 0.037 MBq/m^2 and 0.074 MBq/m^2 respectively. The Polessie State Radioecology Reserve (PSRER) in southern Belarus is one of the most contaminated regions with associated total inventory estimates of 2.5 x 10^9 MBq of ^{137}Cs and 0.18 x 10^9 MBq of ^{90}Sr (Izrael and Bogdevich, 2009). Contamination is spatially highly heterogeneous over distances of 10's of meters or less while significant contamination is also found in the tree canopy and vegetation and in aquatic systems of the area. A general overview of ^{137}Cs levels in the PSRER is presented in Figure 1.

…….Insertion point for Figure 1…….

Figure 1. Spatial distribution of the estimated ^{137}Cs inventory (kBq m^2) across the Polessie State Radioecology Reserve

Cs-137 is usually considered to be the most important long-term anthropogenic contributor to the dose-levels in the environment (Miller, 2007). Its radiological prominence is due to its relatively long half-life of 32 years, its potential to be remobilised through sediment redistribution as it binds strongly to clays and its affinity to be taken in by living tissue given that it readily displaces biological potassium within the body (Povinec et al., 2003). These

factors, amongst others, impart a certain emphasis on the monitoring of levels of this isotope within the environment and such monitoring is especially important in highly contaminated areas such as those of the PSRER where considerable efforts have been expended in establishing the spatial distribution and environmental behaviour of this and other nuclides (see for example Kudelsky,et al., 1996; Knatko et al., 1996; Guermentchuk et al., 1997; Sokolik et al., 2001; Yoschenko et al., 2006).

Monitoring of ^{137}Cs in soils is conventionally achieved by either of two approaches. The first consists of extracting discrete samples or cores from a site and measuring the activity of either the whole sample or of individually sliced samples representative of different depths using laboratory based gamma-ray spectrometers (Tyler, 2008). Although precise information as to the ^{137}Cs depth penetration can be obtained using this method, the resources it takes to obtain, prepare and count individual samples results in spatial coverage being limited and spatial heterogeneities may not always be captured (Tyler et al., 1996a). Estimates of ^{137}Cs penetration down the soil column are particularly important for two reasons. Firstly, knowledge of depth distribution can contribute greatly to remediation strategies and decisions on subsequent site use. Secondly, depth distribution can influence the environmental behaviour of ^{137}Cs particularly with regards to surface remobilisation.

The environment of the PSRER constitutes an interesting problem with respect to how high resolution mapping of contaminant ^{137}Cs can be conducted. The territories not covered by forest (basically abandoned agricultural lands) constitute 38.0 % and non-agricultural unforested lands occupy 9.3 %. Road coverage is sparse and the terrain is generally rugged. While topographically flat, the area has local depressions and elevations as well as a variety of watercourses and bodies (both natural and man-made) in addition to extensive seasonally flooded areas. In general, much of the area is inaccessible by vehicle and can be considered as difficult terrain. In light of the above considerations, the development of a man portable gamma-ray spectrometry system capable of accurate high spatial resolution ^{137}Cs mapping of contamination patterns is paramount (Plamboeck et al., 2006). Within the PSRER, due to spatial hetergeneity ^{137}Cs activity the capability to map changes over metres to tens of metres would provide significant improvement in spatial resolution compared to current approaches.

1.1. In Situ Gamma-ray Spectrometry of ^{137}Cs and Depth Estimation.

The fundamentals of gamma-ray spectrometry can be found elsewhere, for example Knoll (2010). The principle of *in situ* gamma-ray spectrometry is the placing of a suitable instrument above the ground and making a measurement over a specified time period. The resultant measurement offers information as to the localised radiation field through the differential measurement of gamma-rays that interact with the active volume of the detector. Critically, the energies of individual gamma-rays are recorded and accumulated into a differential energy spectrum. Estimating the ^{137}Cs inventory (Bq m^{-2}) directly from the count rate under the characteristic ^{137}Cs 662 keV photopeak is not always a straightforward task given that a number of factors can significantly change the count rate. Ground curvature (Laedermann et al., 1998) and the influence of trees and other vegetation (Gering et al., 2002) can introduce a considerable amount of uncertainty. However, the primary source of uncertainty often arises when significant changes in depth distribution are encountered, as considerable variations can alter the count rate by orders of magnitude (Sowa et al., 1989). Besides altering the count rate, changes in depth distribution can also change the detector's Field of View (FoV) and can have an influence on the spatial response of single measurements. The FoV of a detector can be defined as the effective volume of soil being sampled and is often characterised by the lateral distance or radius from the detector over which the sampling area extends to (Tyler et al., 1996a). Problems can arise when contamination is highly associated with the soil surface, following fresh deposition, reducing the detectors ability to resolve small scale localised heterogeneity given that the FoV for a detector at 1 m above the ground is greater than 70 m radius. Moreover, at this scale topographic anomalies become important in defining the FoV. Nevertheless, Chernobyl deposition has aged over 30 years and much of the contamination is understood to have penetrated sufficiently into the soil column (Smith and Beresford, 2002). This process should have led to reduction in the FoV for a detector at 1m above the ground to approximately less than 10 m (Tyler et al., 1996a). A further way to reduce the FoV is to operate detectors at a nominal height of 0.1 m, which should reduce the FoV down to between 2 to 5 m.

Importantly, prior to any inventory estimations the count rate must be corrected for the appropriate depth distribution and the influence of the FoV must also be considered prior to interpolation mapping. The peak-to-valley ratio (PTV) provides a means of performing this task through spectral information alone (Zombori et al., 1992). PTV has been widely used to

estimate the burial depth distribution of ^{137}Cs and improve the overall accuracy of inventory estimations (Feng et al., 2012; Gering et al., 1998; Hillmann et al., 1996; Tyler, 2004). Tyler et al (1996b) puts forward a particularly visual description of the physical processes that the PTV method is developed upon. In summary, the PTV is the ratio between the number of full energy and forward scattered photons (Figure 2). Forward scattered photons are essentially photons that have lost a small amount of energy whilst exiting the soil and can be located in the "valley" region of the spectrum between the full energy peak at 662 keV and the Compton edge at 480 keV (Figure 2b). Importantly, the greater the depth at which a source is present (Figure 2a), the higher is the probability of photons undergoing forward scattering and occupying the valley region, leading to an increase in valley height and a decrease in the PTV (Figure 2c).

The PTV method can be applied to any detector of adequate energy resolution (Kastlander and Bargholtz, 2005; Tyler, 2004). At present, two of the most commercially widely viable available scintillators that are eminently suitable for portable field operations and that offer high enough energy resolution to measure ^{137}Cs are sodium iodide (NaI:Tl) and lanthanum bromide (LaBr:Ce) (Guss et al., 2010). Of these two, NaI:Tl has been the workhorse of *in situ* and mobile gamma-ray spectrometry for a number a decades as it is relatively cheap, robust and provides acceptable energy resolution (~7% at 662 keV). LaBr:Ce on the other hand is a relatively novel scintillator providing superior energy resolution (2.5% at 662 keV) and higher energy efficiency due to its higher density (5.1 g cm^{-3}) compared to NaI:Tl (3.7 g cm^{-3}). LaBr:Ce does contain an intrinsic background component that can deteriorate the signal to noise ratio especially at low count rates (Nilsson et al., 2014). Another key limitation of LaBr:Ce is that it costs almost an order of magnitude significantly more than NaI:Tl. There have been a relatively large number of studies comparing the performance of NaI:Tl and LaBr:Ce through theoretical or experimental means (Guss et al., 2010; Iltis et al., 2006; Milbrath et al., 2007). Nonetheless, limited comparisons have been undertaken in the field (Duval and Arnold, 2013; Nilsson, 2010) and furthermore only a subset of these have pertained to the measurement of ^{137}Cs (Nilsson et al., 2014).

……Insertion Point for Figure 2……

Figure 2. The relationship between changes in depth distribution (β) and the peak-to-valley ratio observed in a 71 × 71 mm sodium iodide detector. A) Normalised depth distributions

for the same inventory ; B) Peak normalised spectra for different β values demonstrating the relative increase in valley counts with increasing burial; C) A straight-forward regression between calibrated peak-to-valley ratio and β value.

The overarching aim of this investigation is to compare NaI:Tl and LaBr:Ce detector systems for the purposes of characterising spatial ^{137}Cs contamination including its vertical depth distribution at high spatial resolution using one second acquisition times within the PSRER.

2. Methodology

2.1. Field Sites.

The selected sites within the PSRER were topographically flat over areas of 50 m in diameter, the centre of each site being marked with a square area of the size 100 m^2. Each site was specifically chosen to be as homogeneous as possible. As a general indicator of the conditions of the site, the gamma dose rate was recorded with an AT6130 Radiation Monitor (Scientific and Production Enterprise ATOMTEX, Belarus) at each corner and in the centre at a height of 1 m and soil samples were taken at the same points. The location and ambient dose rates over the five sites were as follows: Site 1, a soddy podzolic soil at N 51º33′07,9″ E 029º55′26,1″ (2.21 to 2.50 µSv/h); Site 2, a sandy soil at N 51º33′17,1″ E 029º55′12,1″, (0.29 to 0.35 µSv/h); Site 3, an organic peat soil at N 51º32′54,7″ E 029º55′52,2″ (1.55 to 1.73 µSv/h); Site 4, a regularly flooded, mineral floodplain soil at N 51º31′45,2″ E 029º56′07,5″ (0.52 to 0.89 µSv/h); Site 5, a mineral, ploughed soil at N 51º47′11,8″ E 030º01′16,8″ (0.25 to 0.39 µSv/h). A standard cylindrical corer of 4 cm in diameter and 20 cm extent was used to take cores, each divided into the following increments: 0-3 cm, 3-6 cm, 6-10 cm, 10-15 cm, 15-20 cm. All layers of the same depth from the five cores were bulked and homogenized for gamma-spectrometry. The preparation of soil samples for the radioanalytical measurements included air drying and homogenization by mixing and sieving (2 mm aperture). After weighing, a subsample was transferred to the analytical geometry for counting. A HPGe (Canberra, Be5030, carbon fibre window, 50% rel. eff.) detector was used for ^{137}Cs determination. Count times varied from 6000 to 80000 sec. Statistical uncertainties for the photo peak of ^{137}Cs were less than 5 %. Details as to ^{137}Cs contamination levels at the five test sites are provided in Table 1. For further site information and detailed photographs of the sites refer to Dowdall et al., (2015).

2.2. Gamma-ray Spectrometry System

A 71 (Ø) × 71 mm NaI:Tl and 71 (Ø) × 71 mm LaBr:Ce detectors (both made by Saint Gobain) were connected to individual Ortec digiBases recording a 1024 channel spectral every second using Ortec's Maestro software (ORTEC, 2005). Accompanying each spectrum, GPS coordinates were recorded using an SX Blue II differential GPS, with a resolution of 0.6 m. The software used to combine spectral measurements and spatial coordinates was built

within the JAVA framework and was able to provide real-time feedback on count rates in specified windows. To avoid significant spectral drift occurring, Maestro's gain stabilisation software was operated on the 662 keV peak. In order to capture local inhomogeneities, the detectors were to the operators best abilities held at a constant height of 0.1 m from the ground at all times to narrow the field of view. This was expected to deviate by 0.1 m either way. The shape of the spectrum was assumed not to change significantly therefore, only the count rate was altered according to the changing field of view and calculated through a deterministic model; this was built in as an uncertainty following Monte Carlo simulations. A walking speed of approximately 0.5 m s^{-1} and transect spacing of 0.5 to 1 m was maintained throughout the surveys. Approximately 10 m outside of the test site area were measured in addition to the areas inside the test sites.

2.3. Monte Carlo Simulations

The individual instruments were calibrated using Monte Carlo Simulations (MCS). MCS were preferred over analytical calibration given that the relationship between PTV and changes in ^{137}Cs depth distribution could be modelled with greater precision compared to a limited number of soil core data (Likar et al., 2000). MCS are widely used to estimate detector responses as radiation transport is probabilistic by nature and very difficult to resolve use deterministic approaches (Stromswold, 1995). Hence, by tracking individual particles, through repeated random sampling of well-defined probability distributions a complex problem can be addressed (Maučec et al., 2009).

284

285 Table 1. Inventories, bulk soil density, soil characteristics and depth profiles of ^{137}Cs at each
286 of the five sites.
287

Soil characteristics	Layer	^{137}Cs Bq/kg	% of Total ^{137}Cs Inventory
Soddy podzolic	Site 1		
	0-3 cm	41450+/-8290	66.1+/-13.2
	3-6 cm	15350+/-3070	28.8+/-5.8
	6-10 cm	1360+/-270	3.6+/-0.7
	0-15 cm	314+/-72	1.1+/-0.3
	15-20 cm	92+/-27	0.3+/-0.1
	Bulk density / ^{137}Cs Inventory		1.62 g/cm^3 / 2414 kBq/m^2
Sandy	Site 2		
	0-3 cm	876+/-175	24.0+/-4.8
	3-6 cm	814+/-163	19.4+/-3.9
	6-10 cm	693+/-139	22.6+/-4.5
	0-15 cm	813+/-163	33.4+/-6.7
	15-20 cm	16+/-8	0.6+/-0.3
	Bulk density / ^{137}Cs Inventory		1.77 g/cm^3 / 215 kBq/m^2
Organic peat	Site 3		
	0-3 cm	33380+/-6675	38.7+/-7.7
	3-6 cm	16000+/-3200	30.1+/-6.0
	6-10 cm	5910+/-1180	17.3+/-3.5
	0-15 cm	2740+/-550	10.0+/-2.0
	15-20 cm	947+/-189	3.9+/-0.8
	Bulk density / ^{137}Cs Inventory		1.15 g/cm^3 / 1672 kBq/m^2
Mineral floodplain	Site 4		
	0-3 cm	41810+/-8360	56.6+/-11.3
	3-6 cm	8665+/-1733	22.2+/-4.4
	6-10 cm	3076+/-615	13.4+/-2.7
	0-15 cm	940+/-189	5.9+/-1.2
	15-20 cm	292+/-65	1.8+/-0.4
	Bulk density / ^{137}Cs Inventory		1.23 g/cm^3 / 1178 kBq/m^2
Ploughed mineral	Site 5		
	0-3 cm	2114+/-423	17.8+/-3.6
	3-6 cm	2147+/-435	15.3+/-3.1
	6-10 cm	2164+/-433	20.6+/-4.1
	0-15 cm	2235+/-447	24.9+/-5.0
	15-20 cm	1814+/-362	21.5+/-4.3
	Bulk density / ^{137}Cs Inventory		1.55 g/cm^3 / 644 kBq/m^2

The software package Monte Carlo N-Particle 5 (MCNP5) was used to obtain spectral responses to recover PTV (Briesmeister, 1993). In individual MCS, a basic geometry encompassing the detector, soil column and air filled with constituent materials were described through input cards (Figure 3).

……Insertion Point for Figure 3……..

Figure 3. MCNP setup and method used to derive PTV from an exponential distributed source.

Descriptions of the starting source were also given to MCNP5, alongside F8 tally instructions that captured the differential energy spectrum within the simulated detector's active volume. Given that the PTV is generated using energies considerably higher than those significantly affected by the photoelectric effect and backscatter (>350 keV), Beck et al. (1972) a standard soil composition was used. All nuclide decay data was acquired from the National Nuclear Data Centre (2013).

Validated detector geometries utilised in previous studies (Varley et al., 2015a) were used to derive spectral responses for 71 (Ø) × 71 mm NaI:Tl and LaBr:Ce detectors. Varley et al., (2015a) reported good agreement between MCS and experimental benchmark results collected from doped-concrete calibration pads (1 m^2). The code making up the detector geometries was modelled on manufactures specification provided by Saint Gobain along with receipt of detectors. Detector models encompassed the active volume, its outer canning, a simplified photomultiplier tube and the PVC plastic piping used to house the detection unit (Figure 3). The simulated contamination was an unbiased source of 0.662 MeV photons and the geometry was truncated just above the detector where beyond this point all particles were killed to maximise computer time. No specific reduction variance techniques were used such as Russian roulette.

To optimise the geometry of the simulation, adjoint calculations were utilised to establish the necessary limits or effective FoV of the detector to the source (Varley et al., 2015b). A conservative extent for the surface layer (0-0.01 m) was adopted (25 m) and successively deeper layers were established in the same manner. A Gaussian function was fitted to the

adjoint results that included 99.9 % of the total photons. Importantly, MNCP5 does not take into consideration pile-up effects in the electronics of the scintillator for instance when chance coincidence is encountered (Lindstrom and Fleming, 1995). This phenomenon within environmental spectra can significantly alter the shape of the spectrum at high count rates leading to a smearing of the spectrum and importantly removing counts from the full energy peak to a higher energy channel when combined with lower energy photons (Mowlavi and Hadizadeh Yazdi, 2011). Pile-up can be modelled using a Monte Carlo regime if the spectrum is accurate enough across all energies. However, it was accepted that the lower energy part of the spectrum could not be modelled accurately due to uncertainties associated with the photoelectric effect which is driven by the chemical composition of the soil. Therefore no attempt was made to model this occurrence through Monte Carlo methods. Yet, full energy photon losses in the field were not expected to exceed 0.5 % even at the highest count rates observed. This was established by monitoring the smearing of photons to higher energies.

To achieve spectral responses to a variety of depth distributions and inventories, MCS were simulated at discrete 10 mm depth intervals down to a depth of 70 g cm^{-2} (Figure 3). Beyond 70 g cm^{-2} it was found that contributions to PTV were infinitesimal even for large β values. To form the spectral response for a given value of β and inventory, spectral contributions from each 10 mm slice were weighted in accordance with the appropriate exponential function value (see Eqn [1]). This approach not only permitted the PTV to be defined at a higher depth resolution but also improved counting statistics for later regression models. The reason for this is that the maximum number of particles in MCNP5 (2×10^9) could be run in each simulation effectively increasing source density without repeated random number sampling (Briesmeister, 1993).

Environmental spectra obtained from the test sites contained contributions from the natural radioelements: ^{40}K and the ^{238}U and ^{232}Th series. Although spectral inputs from the natural nuclides were small in comparison to ^{137}Cs, contributions to the valley region were found to influence the PTV particularly at low ^{137}Cs photon fluxes. Therefore, straightforward uniform distributions for the natural radioelements were included as separate MCS (Thummerer and Jacob, 1998).

355 *2.4. Vertical Distribution of ^{137}Cs*

356 In the first decade or so following Chernobyl, many early studies that used field gamma-ray
357 spectrometry to measure ^{137}Cs at undisturbed sites tended to a adopt an exponential function,
358 whereby the activity of contamination was assumed to decrease exponentially with increasing
359 depth as the heavily concentrated ^{137}Cs source on the surface gradually penetrated into the soil
360 column (Hillmann et al., 1996). A number of studies have confirmed this in Belarus and
361 PSRER (Askbrant et al., 1996; Ivanov et al., 1997) However, more recent observations from
362 other areas of Europe have shown the exponential function to break down as the source
363 further penetrates into the soil column and fresh relatively uncontaminated soil buries
364 contamination to form a subsurface maximum (Almgren and Isaksson, 2006; Bernhardsson et
365 al., 2015). However, the most recent study conducted in the PSRER suggests that the
366 exponential function is perhaps still the most appropriate (Dowdall et al., 2017). There reason
367 are three reasons that might explain this outcome. Firstly, the PSRER in comparison to other
368 parts of Europe, where many of the aforementioned studies were conducted, receives
369 relatively low annual rainfall possibly limiting penetration. Secondly, the primary mode of
370 contamination deposition at the time of the accident was dry deposition rather than wet
371 deposition reducing initial infiltration (Drozdovitch et al., 2013). Finally, within a 30 km
372 radius of the ChNPP, radiocaesium was thought to be highly associated with fuel fragments
373 significantly affecting its physiochemical form and ultimately its mobility (Smith and
374 Beresford, 2002).
375
376 These facts combined with the knowledge that the PSRER has not been disturbed to any great
377 extent in over 30 years, therefore justify an exponential decay function to be used in the
378 modelling of the ^{137}Cs depth distribution in this environment (ICRU, 1994). Wherein the
379 activity (A_m) (Bq kg^{-1}) of the soil changes with mass per unit area (ζ) (g cm^{-2}) (Eqn [1]).
380
381 $$A_m(\zeta) = A_{m,0} \cdot e^{(-\zeta/\beta)} \quad [1]$$
382
383 Notice, mass per unit area is preferred over physical depth (cm) as it takes into account
384 density (ρ), which generates a better approximation of shielding and thus permits inventory
385 (Bq m^{-2}) to be calculated more accurately (Eqn [1]). The relaxation mass per unit area (β)
386 relates the rate at which the surface activity (A_0) decreases with mass depth. Resultantly, β

values approaching 0 will define surface contamination whilst uniform contamination will approach ∞.

2.5. Peak and Valley Calculation

The first step in calculation of the PTV was identification of a peak within the correct area of a spectrum obtained in the field. The gain stabilisation software, in the vast majority of cases, centred the 662 keV peak in the correct channel, however small amounts of spectral drift occurred during the survey. To ensure the peak (NaI:Tl = 586.8-737.2 keV; LaBr:Ce = 618.3-705.7 keV), valley (NaI:Tl = 496.5-583.8 keV; LaBr:Ce = 498.7-615.3 keV) and background (NaI:Tl = 740.2-755.3 ; LaBr:Ce = 708.7-726.8 keV) region of interests remained the same between spectra, a Gaussian function was fitted to the peak, the maximum of which could then act as a more precise energy calibration. Thereafter, the background under the peak was estimating using a straightforward linear model fitted to five channels either side of the base of the peak. The background was then subtracted and a second Gaussian function was fitted and integrated to calculate the area. The valley height was calculated by subtracting the area to the high energy side of the peak from the valley region (Tyler, 2004). This routine was written using the base features of the R statistical package (R Core Development Team, 2016).

2.6. Data Generation

For each detector a calibration dataset was generated, comprised of 1000 spectral responses, derived through randomly sampling input β and inventory parameters and applying them to the MCS dataset. The calibration dataset provided spectra with relatively low uncertainty to facilitate fitting of statistical models. An independent dataset (of 2000 spectral responses) was also formed. This dataset, known as the cross-validation dataset, provided a means of assessing performance through Root Mean Square Error (RMSE) for β and inventory estimates. The same modelling constraints applied to the calibration dataset were used to form the cross-validation dataset, but with the addition of the natural radionuclides (^{40}K, ^{238}U and ^{232}Th series) and Poisson noise generated from the one second counts. A similar bootstrapping subroutine of MCS has proven valuable in previous studies to sample both background and source populations when *a priori* knowledge is not available (Varley et al., 2015b).

Model parameters (Table 2) were chosen to be representative of the variation that could take place within the PSRER environment. Simulated inventories were markedly higher than those at the five test sites, but it was deemed necessary to develop an approach that could be used for higher deposition densities. Additionally, a maximum β value of 100 was chosen as it was discovered through preliminary investigations that larger values contributed negligible counts into the valley regions and would be almost impossible to differentiate. In any case, β values above 100 make very little difference to final inventory estimations and will have negligible contribution if dose rate calculations are performed (ICRU, 1994).

Table 2. Parameters used to construct a synthetic dataset.

Parameter	Minimum	Mean	Median	Maximum
^{137}Cs inventory (kBq m^{-2})	7.2	2479.3	282	86962.2
β (g cm^{-2})	0.13	18.3	7.6	100.0
^{40}K inventory (kBq m^{-2})	28.2	226.7	222.6	565.2
^{238}U inventory (kBq m^{-2})	7.1	17.5	16.7	42.39
^{232}Th inventory (kBq m^{-2})	7.1	19.3	18.4	42.4

2.7. Calibration Curves

To establish appropriate calibration curves to estimate β and inventory for each detector, a linear model was fitted to the respective calibration datasets through a conventional least-squares fitting regime (Crawley, 2012). The relationship between explanatory and response variables was found to be log-linear whereby both response (β) and explanatory (PTV) variables were logarithmic. Formulation of the depth model was performed by regressing PTV against β, where β_0 is the point at which PTV is equal to zero and βs is the slope factor applied to PTV (Eqn [1])

$$log(\beta) = \beta_0 + \beta_s \cdot log(PTV) \quad [2]$$

The inventory model was estimated by calculating the calibration coefficient *C*, by dividing the inventory *(A)* by the number of counts in the full energy peak *(N_p)* (Eqn [3]). *C* could then be regressed against the PTV to generate the intercept (C_0) and the slope factor (C_s) (Eqn [4]).

$$C = A/N_p \quad [3]$$

$$log(C) = C_0 + C_s \cdot (PTV) \quad [4]$$

Applied to field estimates the PTV can be used to derive *C*, which need only be multiplied by N_p to estimate inventory (Tyler et al., 1996b).

2.8. Detector-core Comparisons

To develop a firm basis for statistical comparison with the soil core results, all spectra obtained inside the sites were isolated using a georeferenced polygon, run through the calibrated models and then aggregated to form a median and interquartile ranges. On average approximately 600 spectra were collected at each site. Median and interquartile ranges were preferred over the mean and standard deviation as estimates were found to be highly skewed. Core inventory estimates were the sum of the total activity of the core multiplied by the reciprocal of the total core diameter (m^2). Uncertainties were principally based on counting uncertainty. Derivation of β for core data was performed by using a least-squares fitting regime on the function described in Eqn [1]. Uncertainties were derived by Monte Carlo simulation.

3. Results and Discussion

3.1. Statistical Modelling of Monte Carlo Simulations

Statistically significant relationships (R^2 values greater than 0.93; $p < 0.05$) were found for all models derived from the calibration datasets (Table 3). Model parameter values are similar between detectors, suggesting that the detectors respond in a similar manner to an extended environmental ^{137}Cs source.

Table 3. Parameter and R^2 values for depth and inventory models for lanthanum bromide and sodium iodide detectors.

		Depth model			Inventory model			
Detector	B_0	B_s	R^2	*RMSE*	C_0	C_s	R^2	*RMSE*
LaBr:Ce	1579.71	0.97	0.93	19.32	10.23	0.98	0.98	407.21
NaI:Tl	1423.46	0.97	0.94	22.04	11.92	0.98	0.99	483.85

Based on RMSE values on validation datasets in which Poisson noise and natural background were introduced, LaBr:Ce (407.21 kBq m^{-2} and 19.32 g cm^{-2}) marginally outperformed NaI:Tl (483.85 kBq m^{-2} and 22.04 g cm^{-2}) (Table 3). LaBr:Ce would at this stage appear to offer increased performance. Nonetheless, to investigate the response of each detector further the average uncertainty made on inventory and β estimates, as a function inventory, has been presented (Figure 4).

……Insertion Point for Figure 4……

Figure 4. A) Percentage error associated with inventory estimates as a function of inventory for: lanthanum bromide (purely based on peak counts), lanthanum bromide (peak-to-valley corrected) and sodium iodide (peak-to-valley corrected) B) Percentage error associated with β estimates as a function of inventory for lanthanum bromide (peak-to-valley corrected) and sodium iodide (peak-to-valley corrected).

Firstly, the advantage of using PTV corrected data can be realised when compared to uncorrected data derived from peak counts (Figure 4A). At inventories greater than 100 kBq m^{-2}, there is clear divergence in the percentage error on inventory estimates between corrected and uncorrected LaBr:Ce results, which becomes significantly larger as inventory increases. This occurrence can be explained through counting statistics. For example, at low peak count rates (typically of the order of a few hundred) the uncertainty associated with the calculation of PTV is large enough that it does not aid in the estimation of inventory; the highest source of uncertainty in this instance will be associated with the valley height calculation. However, as count rates rise with increasing contamination, and the valley calculation becomes more reliable, the PTV correction significantly decreases the percentage error associated with inventory estimation.

Reinforcing the RMSE values (Table 3), corrected NaI:Tl and LaBr:Ce would appear to produce similar percentage error across the inventory range (Figure 4A). Yet, at inventories less than ~1500 kBq m^{-2}, NaI:Tl exhibits an advantage of ca. 5% lower percentage error than LaBr:Ce. Above ~1500 kBq m^{-2}, LaBr:Ce would appear to improve on NaI:Tl by approximately 1%. This fact is associated with the intrinsic background contained with the LaBr:Ce active volume. Therefore, at lower count rates, the signal to noise ratio is lower than that of NaI:Tl, nonetheless, when count rates exceed a roughly thousand or more the improved energy resolution deems it superior. A similar aspect is observed when analysing percentage error associated with β estimates as a function of inventory (Figure 4B). Note, there is a similar crossover at approximately ~1000 kBq m^{-2}, but in this case the advantage above this value is clearer for the LaBr:Ce detector (~10%). Interestingly, percentage error on β values are seen to plateau for both detectors at densities around 4000 kBq m^{-2}. This possibly represents the absolute limit of detection where very little improvement on depth estimate can be made using the devices, this is due to the sensitivity of the ratio at greater values of β.

3.2. Application to the Reference Sites

Core results confirmed that there was a large variation in both the depth distribution and total inventory across the five test sites (Figure 5). General patterns included a clear surface association of contamination at the high activity organic-rich sites (1, 3 and 4) and sites with

significant vertical penetration: sites 2 (sandy) and 5 (ploughed). Applying the models developed from MCS to data collected over the test sites yielded encouraging results. Generally, there was good agreement between core and detector inventory estimates particularly for sites 1, 2 and 4 with less than 25 % difference between core and detector estimates (Figure 6A).

……Insertion Point for Figure 5……

Figure 5. Inventory depth distributions derived from soil cores extracted from the five GAMFAC sites. Uncertainties are one standard deviation and based on counting statistics.

Results are very similar for both detectors for all of the sites confirming earlier percentage error investigations (see Figure 4A). The detectors struggled equally to characterise the inventory at sites 2 and 5 where differences of ca. 53 % and 45 % were encountered (see Figure 6A). It became clear that this method may be limited at sites were the level of contamination is relatively low and at greater depths when operating with one second count times. To lower the uncertainty, it might be appropriate to lengthen the count time or, alternatively, conduct slower traverses and increasing the spatial density of spectra, which could, retrospectively, be summed to improve statistics. It must also be noted that remote measurements tend to only sample the top 20 cm or so of soil, much of the contamination at these sites is below this range and most possibly beyond the detection capabilities of these instruments (see Figure 4A). In addition, it may be argued that these sites could be described as a having subsurface maxima (~20 g cm^{-2}), which the exponential model would have struggled to accurately characterise (see Figure 5). Alternate more flexible models, for example the one described by Hillman et al. (1996) or (Almgren and Isaksson, 2006) might be more appropriate in this case. This could have been more representative of the PTV values found in the field and reduced the uncertainty associated with final inventory estimates.

…… Insertion Point for Figure 6 ……

Figure 6. Median and interquartile range values for inventory (A) and β (B) estimates for the five GAMFAC sites for lanthanum bromide and sodium iodide compared to core results.

An example of how complex the spatial distribution of ^{137}Cs in the PSRER can be is provided, whereby inventory and β values obtained using NaI:Tl from site 2 and the area surrounding have been smoothed using universal kriging (Graphical abstract). First of all, notice the reference site chosen on the sand dune (red broken lines) was relatively stable with little variation in inventory and depth confirming it a good choice of reference site to apply static *in situ* systems. However, outside of the isolated site large fluctuations in inventory and depth were witnessed. For instance two relatively large hotspots (5-15 meters in diameter) to the north of the site were estimated to possess more than six times the inventory (~1500 kBq m^{-2}) of the reference site. Due to the geometry and distance away from the reference site these sources would nonetheless have little impact on final calibration measurements taken at the site. Together with greater inventory, β values associated with these hotspot were estimated to be greater than the surrounding area suggesting contamination was deeper in the soil column. This finding could suggest accumulation and penetration of contamination particularly in areas of the topographic depression in the foreground, which was lower in elevation than the sand dune and could potentially accumulate ^{137}Cs through erosion processes. Further investigative studies involving coring and chemical analysis would have to be performed to confirm this hypothesis.

Graphical abstract. Estimated inventory and β obtained for 71 × 71 mm sodium iodide detector for site 2 (red box) and surrounding area. Notice the reference site (red box) is significantly more stable than surrounding areas in terms of depth and activity.

4. Conclusions

The Chernobyl Nuclear power plant disaster has been the single largest nuclear reactor meltdown in our history. Subsequently, highly radioactive material can be found in large areas of Ukraine, Belarus and Russia presenting a considerable remediation challenge that could take decades or even centuries to overcome. An important step in this process is develop methods to characterise the activity and burial depth of ^{137}Cs in high spatial resolution. To this end, a highly practical method has been described and validated against reference sites within the Polessie State Radioecological Reserve in southern Belarus. It was shown that a conventional 71 × 71 mm sodium iodide scintillation detector could exhibit equal performance to a significantly more expensive lanthanum bromide detector of the same size and power requirements. This outcome can be attributed to the intrinsic contamination associated with lanthanum bromide. Depth and activity maps of ^{137}Cs contamination have demonstrated the advantage of the technique applied to the sodium iodide detector. Further application of this approach could significantly support future remediation activities ultimately lowering the risk to human health.

5. Acknowledgements

This work was performed as part of the GAMFAC intercomparison exercise funded by the Nordic Nuclear Safety Research. The authors would like to acknowledge the staff of the Polessie State Radiation Ecology Reserve of Belarus for the organisation of the GAMFAC project and processing of cores. Additonal gratitude must be served to Ms. Elena Almås for her invaluable translation.

627 **References**

628

629 Almgren, S., Isaksson, M., 2006. Vertical migration studies of ^{137}Cs from nuclear weapons
630 fallout and the Chernobyl accident. J. Environ. Radioact. 91, 90–102.
631 doi:10.1016/j.jenvrad.2006.08.008

632 Askbrant, S., Melin, J., Sandalls, J., Rauret, G., Vallejo, R., Hinton, T., Cremers, A.,
633 Vandecastelle, C., Lewyckyj, N., Ivanov, Y.A., Firsakova, S.K., Arkhipov, N.P.,
634 Alexakhin, R.M., 1996. Mobility of radionuclides in undisturbed and cultivated soils in
635 Ukraine, Belarus and Russia six years after the Chernobyl fallout. J. Environ. Radioact.
636 31, 287–312. doi:10.1016/0265-931X(95)00054-E

637 Beck, H., DeCampo, J., Gogolak, C., 1972. In situ Ge(Li) and NaI(Tl) gamma-ray
638 spectrometry. New York. doi:10.2172/4599415

639 Bernhardsson, C., Roof, C.L., Mattsson, S., 2015. Spatial variability of the dose rate from
640 137Cs fallout in settlements in Russia and Belarus more than two decades after the
641 Chernobyl accident. J. Environ. Radioact. 149, 144–149.
642 doi:http://dx.doi.org.ezproxy.stir.ac.uk/10.1016/j.jenvrad.2015.07.009

643 Briesmeister, J.F., 1993. MCNP-A general Monte Carlo N-particle transport code. LA-12625.

644 Center, N.N.D., 2013. Nuclear datasheets. URL http://www.nndc.bnl.gov/ensdf/

645 Crawley, M.J., 2012. The R book. John Wiley & Sons. ISBN-13: 978-0470510247
646

647 Dowdall, M., Bondar, Y., Skipperud, L., Zabrotski, V., Pettersen, M.N., Selnæs, G., Brown,
648 J.E., 2017. Investigation of the vertical distribution and speciation of ^{137}Cs in soil
649 profiles at burnt and unburnt forest sites in the Belarusian Exclusion Zone. J. Environ.
650 Radioact. 175-176, 60–69. doi:10.1016/j.jenvrad.2017.04.009

651 Dowdall, M., Bondar, Y.I., Fristrup, P., Guonason, K., Granstrom, M., Hedman, A., Israelson,
652 C., Jonsson, G., Kjerulf, S., Juul Krogh, S., Mauring, A., Moller, B., Tyler, A.N., Varley,
653 A., Zabrotski, V., 2015. Advanced In-situ Gamma Spectrometry Field Activity
654 Chernobyl (GAMFAC), GAMFAC. Nordic Nuclear Safety Research, Denmark.

655 Drozdovitch, V., Zhukova, O., Germenchuk, M., Khrutchinsky, A., Kukhta, T., Luckyanov,

N., Minenko, V., Podgaiskaya, M., Savkin, M., Vakulovsky, S., Voillequ, P., Bouville, A.A., Voillequé, P., Bouville, A.A., 2013. Database of meteorological and radiation measurements made in Belarus during the first three months following the Chernobyl accident. J. Environ. Radioact. 116, 84–92. doi:http://dx.doi.org.ezproxy.stir.ac.uk/10.1016/j.jenvrad.2012.09.010

Duval, M., Arnold, L.J., 2013. Field gamma dose-rate assessment in natural sedimentary contexts using LaBr3(Ce) and NaI(Tl) probes: A comparison between the "threshold" and "windows" techniques. Appl. Radiat. Isot. 74, 36–45. doi:10.1016/j.apradiso.2012.12.006

Feng, T.C., Jia, M.Y., Feng, Y.J., 2012. Method-sensitivity of in-situ gamma spectrometry to determine the depth-distribution of anthropogenic radionuclides in soil. Nucl. Instruments Methods Phys. Res. Sect. A-Accelerators Spectrometers Detect. Assoc. Equip. 661, 26–30. doi:10.1016/j.nima.2011.09.014

Gering, F., Hillmann, U., Jacob, P., Fehrenbacher, G., 1998. In situ gamma-spectrometry several years after deposition of radiocesium II. Peak-to-valley method. Radiat. Environ. Biophys. 37, 283–291. doi:10.1007/s004110050130

Gering, F., Kiefer, P., Fesenko, S., Voigt, G., 2002. In situ gamma-ray spectrometry in forests: determination of kerma rate in air from ^{137}Cs. J. Environ. Radioact. 61, 75–89. doi:http://dx.doi.org/10.1016/S0265-931X(01)00116-3

Guermentchuk, M.G., Zhukova, O.M., Shagalova, E.D., Matveenko,, I.I. 1997. Radioecological mapping of the territory of Belarus on the base information of radiation monitoring. In: IAEA-TECDOC-980. Uranium Exploration Data and Techniques Applied to the Preparation of Radioelement Maps, Proceedings of a Technical Committee Meeting, International Atomic Energy Agency (IAEA), Vienna. ISSN 1011-4289. Pp. 153-161

Guss, P., Reed, M., Yuan, D., Cutler, M., Contreras, C., Beller, D., 2010. Comparison of CeBr(3) with LaBr(3):Ce, LaCl(3):Ce, and NaI:Tl Detectors. Proc. SPIE-The Int. Soc. Opt. Eng. 7805, 78050L–78050L. doi:10.1117/12.862579

Hillmann, U., Schimmack, W., Jacob, P., Bunzl, K., 1996. In situ gamma-spectrometry

686 several years after deposition of radiocesium .1. Approximation of depth distributions by
687 the Lorentz function. Radiat. Environ. Biophys. 35, 297–303.
688 doi:10.1007/s004110050043

689 International Commission on Radiation Units (ICRU), 1994. Gamm-Ray Spectrometry in the
690 Environmental. International Commission on the Radiation Units and Measurements,
691 7910 Woodmont Avenue Bethesda, Maryland 20814, U.S.A.

692 Iltis, A., Mayhugh, M.R., Menge, P., Rozsa, C.M., Selles, O., Solovyev, V., 2006. Lanthanum
693 halide scintillators: Properties and applications. TRDs Third Millenium Proc. 3rd Work.
694 Adv. Transit. Radiat. Detect. Accel. Sp. Appl. 3rd Work. Adv. Transit. Detect. Accel.
695 Sp. Appl. 563, 359–363. doi:10.1016/j.nima.2006.02.192

696 Izrael, Yu.A., Bogdevich, I.M. (Eds.) 2009. The Atlas of recent and predictable aspects of
697 consequences of Chernobyl accident on polluted territories of Russia and Belarus
698 (ARPA Russia-Belarus) Moscow-Minsk: Infosphere Foundation NIA-Nature.
699

700 Ivanov, Y.A., Lewyckyj, N., Levchuk, S.E., Prister, B.S., Firsakova, S.K., Arkhipov, N.P.,
701 Arkhipov, A.N., Kruglov, S. V., Alexakhin, R.M., Sandalls, J., Askbrant, S., 1997.
702 Migration of 137Cs and 90Sr from Chernobyl fallout in Ukrainian, Belarussian and
703 Russian soils. J. Environ. Radioact. 35, 1–21. doi:10.1016/S0265-931X(96)00036-7

704 Kastlander, J., Bargholtz, C., 2005. Efficient in situ method to determine radionuclide
705 concentration in soil. Nucl. Instruments Methods Phys. Res. Sect. A-Accelerators
706 Spectrometers Detect. Assoc. Equip. 547, 400–410. doi:10.1016/j.nima.2005.03.143

707 Knatko, V.A., Skomorokhov, A.G., Asimova, V.D., Strakh, L.I., Mironov, V.P. 1996.
708 Characteristics of ^{90}Sr, ^{137}Cs and ^{239,240}Pu migration in undisturbed soils of southern
709 Belarus after the Chernobyl accident. J. Environ. Radioact, 30(2): 185-196,
710 http://dx.doi.org/10.1016/0265-931X(95)00011-X
711

712 Knoll, G.F., 2010. Radiation detection and measurement. John Wiley & Sons. ISBN : 978-1-
713 118-02691-5

714 Kudelsky, A.V., Smith, J.T., Ovsiannikova, S.V., Hilton, J. 1996. Mobility of Chernobyl-
715 derived ^{137}Cs in a peatbog system within the catchment of the Pripyat River, Belarus. Sci.
716 Total Environ. 188(2–3), 101-113, http://dx.doi.org/10.1016/0048-9697(96)05162-5
717
718 Likar, A., Omahen, G., Vidmar, T., Martincic, R., 2000. Method to determine the depth of Cs-
719 137 in soil from in-situ gamma-ray spectrometry. J. Phys. D. Appl. Phys. 33, 2825.
720 http://stacks.iop.org/0022-3727/33/i=21/a=323

721 Lindstrom, R., Fleming, R., 1995. Dead time, pileup, and accurate gamma-ray spectrometry.
722 Radioact. Radiochem. 6, 20–27.

723 Maučec, M., Hendriks, P.H.G.M., Limburg, J., de Meijer, R.J., 2009. Determination of
724 correction factors for borehole natural gamma-ray measurements by Monte Carlo
725 simulations. Nucl. Instruments Methods Phys. Res. Sect. A Accel. Spectrometers,
726 Detect. Assoc. Equip. 609, 194–204. doi:http://dx.doi.org/10.1016/j.nima.2009.08.054

727 Milbrath, B.D., Choate, B.J., Fast, J.E., Hensley, W.K., Kouzes, R.T., Schweppe, J.E., 2007.
728 Comparison of LaBr3:Ce and NAI(Tl) scintillators for radio-isotope identification
729 devices. Nucl. Instruments Methods Phys. Res. Sect. A Accel. Spectrometers, Detect.
730 Assoc. Equip. 572, 774–784. doi:10.1016/j.nima.2006.12.003

731 Miller, M.L., 2007. Cesium-137 in the Environment: Radioecology and Approaches to
732 Assessment and Management. NCRP Rep. No.154, Cesium-137 Environ. Radioecol.
733 Approaches to Assess. Manag. 151. ISBN-10: 0-929600-91-6

734 Mowlavi, A.A., Hadizadeh Yazdi, M.H., 2011. Monte Carlo simulation of pulse pile-up effect
735 in gamma spectrum of a PGNAA system. Nucl. Instruments Methods Phys. Res. Sect. A
736 Accel. Spectrometers, Detect. Assoc. Equip. 660, 104–107.
737 doi:10.1016/j.nima.2011.09.022

738 Nilsson, J.M.C., 2010. Using the $LaBr_3$:Ce scintillation detector for mobile γ-spectrometry .
739 Department of Medical Radiation Physics, Lund University (Master's thesis).

740 Nilsson, J.M.C., Östlund, K., Söderberg, J., Mattsson, S., Rääf, C., 2014. Tests of HPGe- and
741 scintillation-based backpack γ-radiation survey systems. J. Environ. Radioact. 135, 54–
742 62. doi:10.1016/j.jenvrad.2014.03.013

ORTEC, 2005. MAESTRO (computer software)

Plamboeck, A.H., Nylén, T., Ågren, G., 2006. Comparative estimations of ^{137}Cs distribution in a boreal forest in northern Sweden using a traditional sampling approach and a portable NaI detector. J. Environ. Radioact. 90, 100–109. doi:10.1016/j.jenvrad.2006.06.011

Povinec, P.P., Bailly du Bois, P., Kershaw, P.J., Nies, H., Scotto, P., 2003. Temporal and spatial trends in the distribution of ^{137}Cs in surface waters of Northern European Seas - a record of 40 years of investigations. Worldw. Mar. Radioact. Stud. 50, 2785–2801. doi:http://dx.doi.org/10.1016/S0967-0645(03)00148-6

R Core Development Team, 2016. R: A language and environment for statistical computing. R A Lang. Environ. Stat. Comput.

Smith, J.T., Beresford, N.A., 2002. Radioactive fallout and environmental transfers. Chernobyl — Catastr. Consequences 35–80. doi:10.1007/3-540-28079-0_2

Sokolik, G.A., Ivanova, T.G., Leinova, S.L., Ovsiannikova, S.V., Kimlenko, I.M. 2001. Migration ability of radionuclides in soil-vegetation cover of Belarus after Chernobyl accident. Env. Int. , 26(3): 183-187. http://dx.doi.org/10.1016/S0160-4120(00)00104-5

Sowa, W., Martini, E., Gehrcke, K., Marschner, P., Naziry, M.J., 1989. Uncertainties of in situ gamma spectrometry for environmental monitoring. Radiat. Prot. Dosimetry 27, 93–101. https://doi.org/10.1093/oxfordjournals.rpd.a080450

Stromswold, D.C., 1995. Calibration facilites for borehole and surface environmental radiation measurements. J. Radioanal. Nucl. Chem. 194, 393–401. 10.1007/BF02038439

Thummerer, S., Jacob, P., 1998. Determination of depth distributions of natural radionuclides with in situ gamma-ray spectrometry. Nucl. Instruments Methods Phys. Res. Sect. A-Accelerators Spectrometers Detect. Assoc. Equip. 416, 161–178. doi:10.1016/S0168-9002(98)00636-6

Tyler, A., 2008. In situ and airborne gamma-ray spectrometry. Radioact. Environ. 11, 407-448. https://doi.org/10.1016/S1569-4860(07)11013-5Tyler, A., Sanderson, D., Scott, E.,

1996a. Accounting for spatial variability and fields of view in environmental gamma ray spectrometry. J. Environ. http://dx.doi.org/10.1016/S1569-4860(07)11013-5

Tyler, A., Sanderson, D., Scott, E., 1996b. Estimating and accounting for ^{137}Cs source burial through in-situ gamma spectrometry in salt marsh environments. J. Environ. http://dx.doi.org/10.1016/0265-931X(95)00098-U

Tyler, A.N., 2004. High accuracy in situ radiometric mapping. J. Environ. Radioact. 72, 195–202. doi:10.1016/S0265-931X(03)00202-9

United Nations Scientific Committee on the Effects of Atomic Radiation (UNSCEAR), 2000. Annex J: Exposures and Effects of the Chernobyl Accident. 115 p.

Varley, A., Tyler, A., Smith, L., Dale, P., 2015b. Development of a neural network approach to characterise ^{226}Ra contamination at legacy sites using gamma-ray spectra taken from boreholes. J. Environ. Radioact. 140, 130–140. doi:10.1016/j.jenvrad.2014.11.011

Varley, A., Tyler, A., Smith, L., Dale, P., Davies, M., 2015a. Remediating radium contaminated legacy sites: Advances made through machine learning in routine monitoring of "hot" particles. Sci. Total Environ. 521-522, 270–279. doi:10.1016/j.scitotenv.2015.03.131

Webster, S.C., Byrne, M.E., Lance, S.L., Love, C.N., Hinton, T.G., Shamovich, D., Beasley, J.C., 2016. Where the wild things are: influence of radiation on the distribution of four mammalian species within the Chernobyl Exclusion Zone. Front. Ecol. Environ. 14, 185–190. http://dx.doi.org/10.1002/fee.1227

Yoschenko, V.I., Kashparov, V.A., Levchuk, S.E., Glukhovskiy, A.S., Khomutinin, Y. V, Protsak, V.P., Lundin, S.M., Tschiersch, J., 2006. Resuspension and redistribution of radionuclides during grassland and forest fires in the Chernobyl exclusion zone: part II. Modeling the transport process. J. Environ. Radioact. 87, 260–278. doi:http://dx.doi.org/10.1016/j.jenvrad.2005.12.003

Zombori, P., Németh, I., Andrâsi, A., Lettner, H., 1992. In-situ gamma-spectrometric measurement of the contamination in some selected settlements of Byelorussia (BSSR), Ukraine (UkrSSR) and the Russian Federation (RSFSR). J. Environ. Radioact. 17, 97–

106. doi:http://dx.doi.org/10.1016/0265-931X(92)90019-P

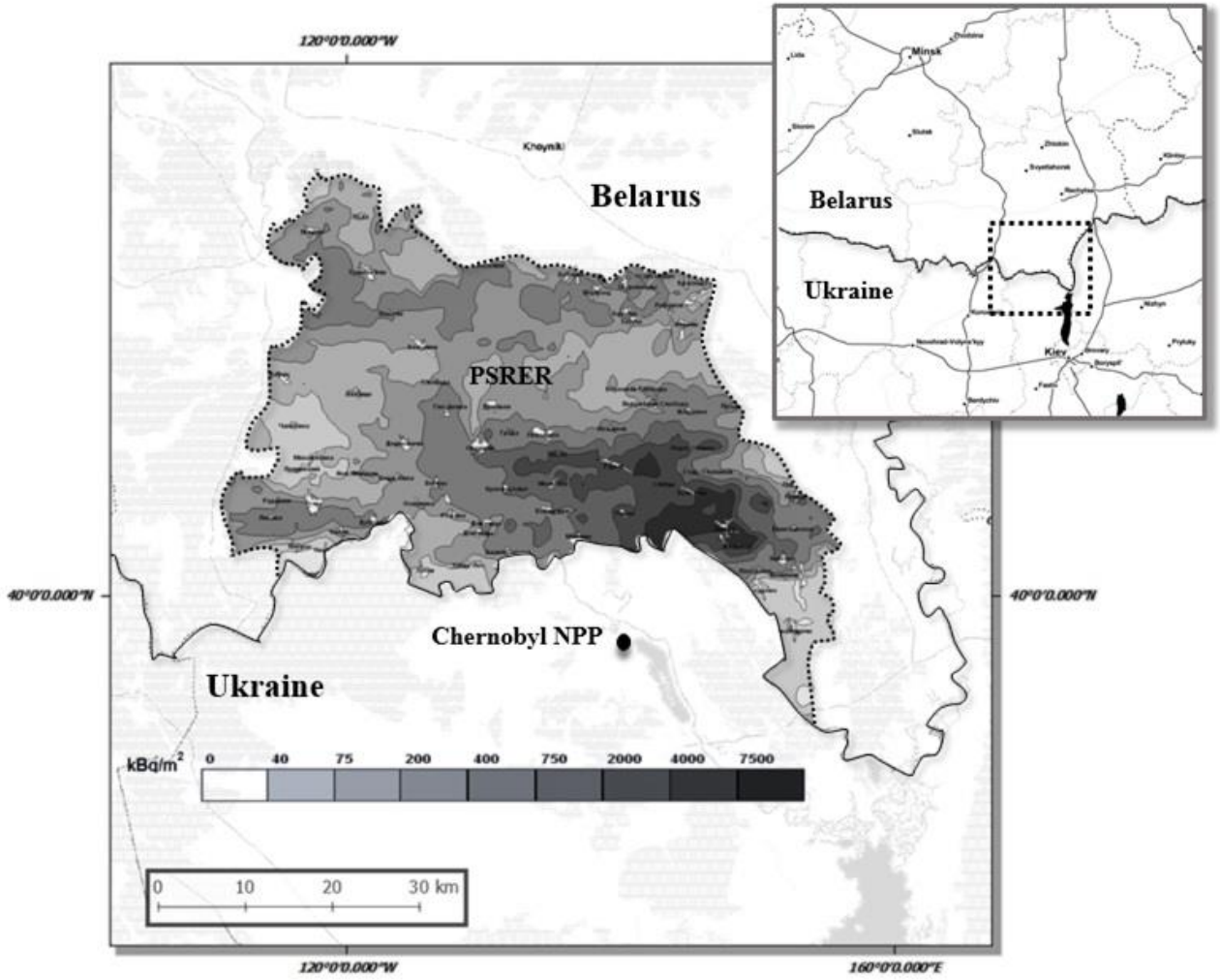

834

835 ***Figure 1***

836

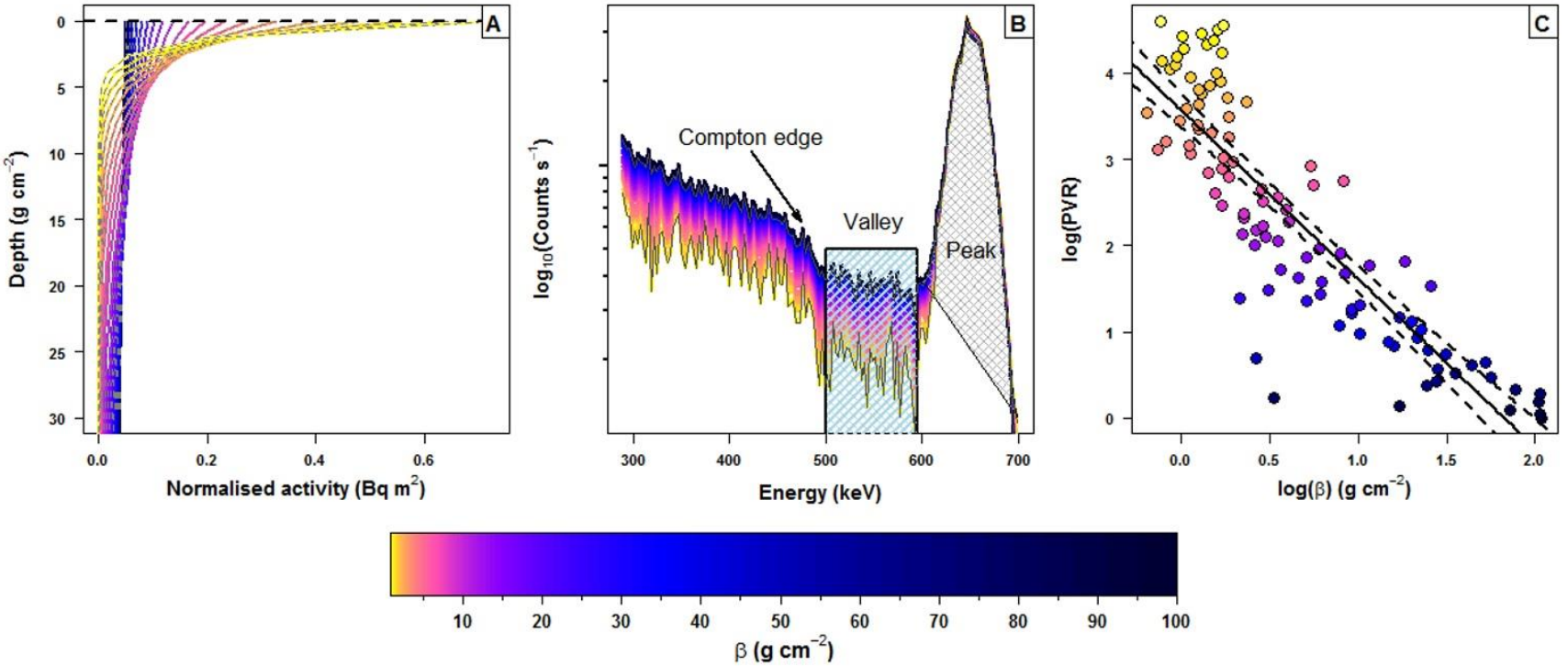

837

838 ***Figure 2***

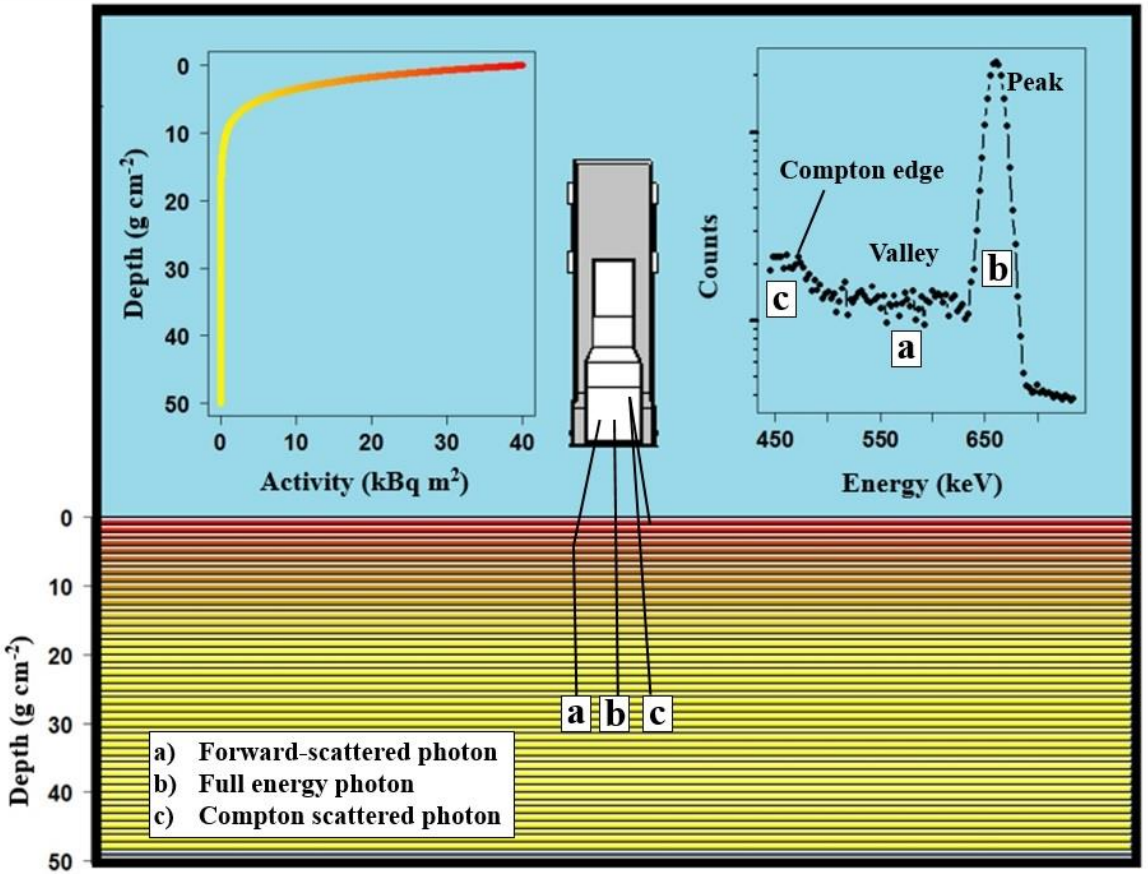
Depth (g cm-2)
0
10
20
30
40
50
Activity (kBq m2)
Counts
Peak
Compton edge
Valley
a
b
c
450
550
650
Energy (keV)
a) Forward-scattered photon
b) Full energy photon
c) Compton scattered photon

Figure 3

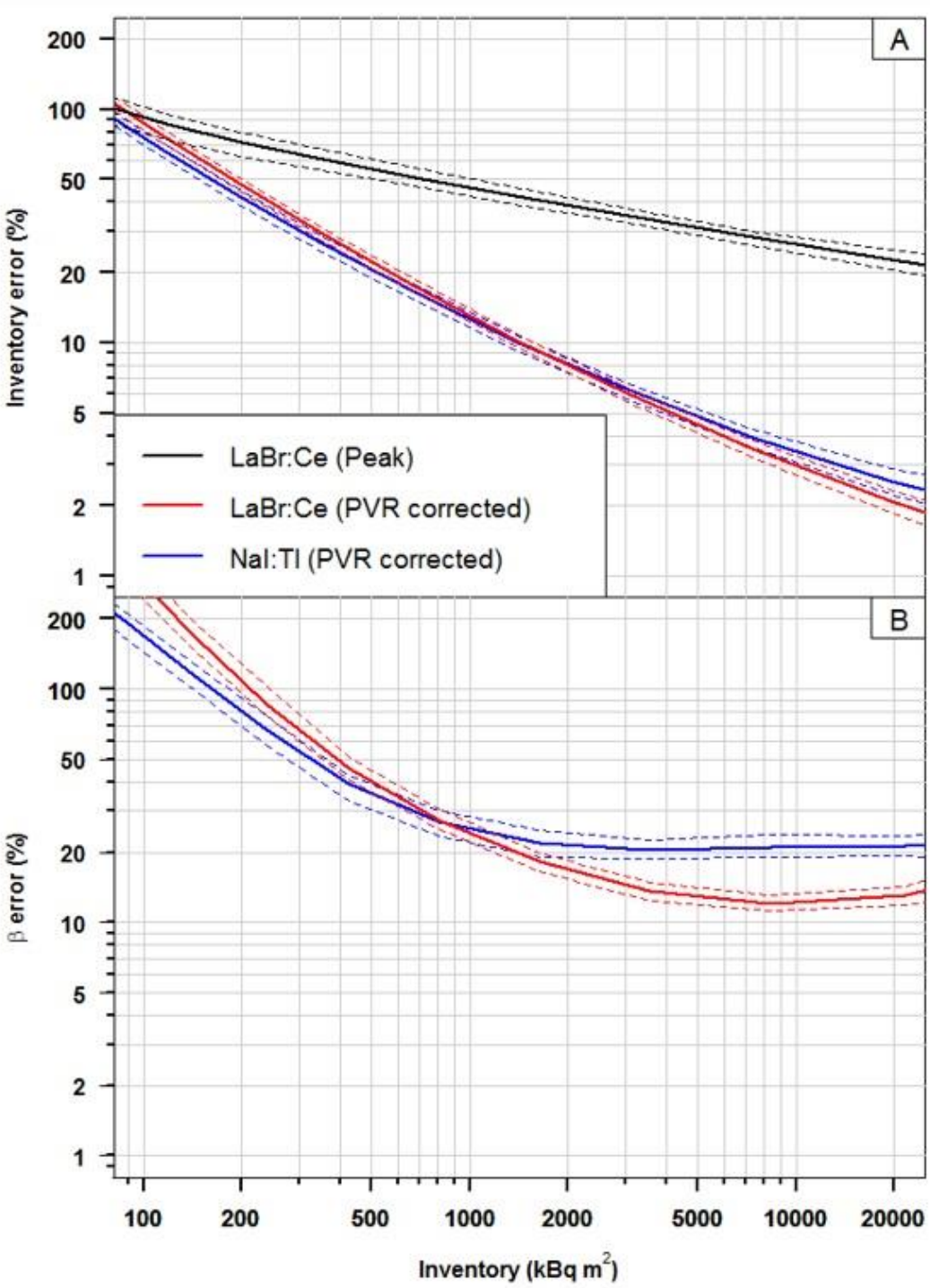

841

842 ***Figure 4***

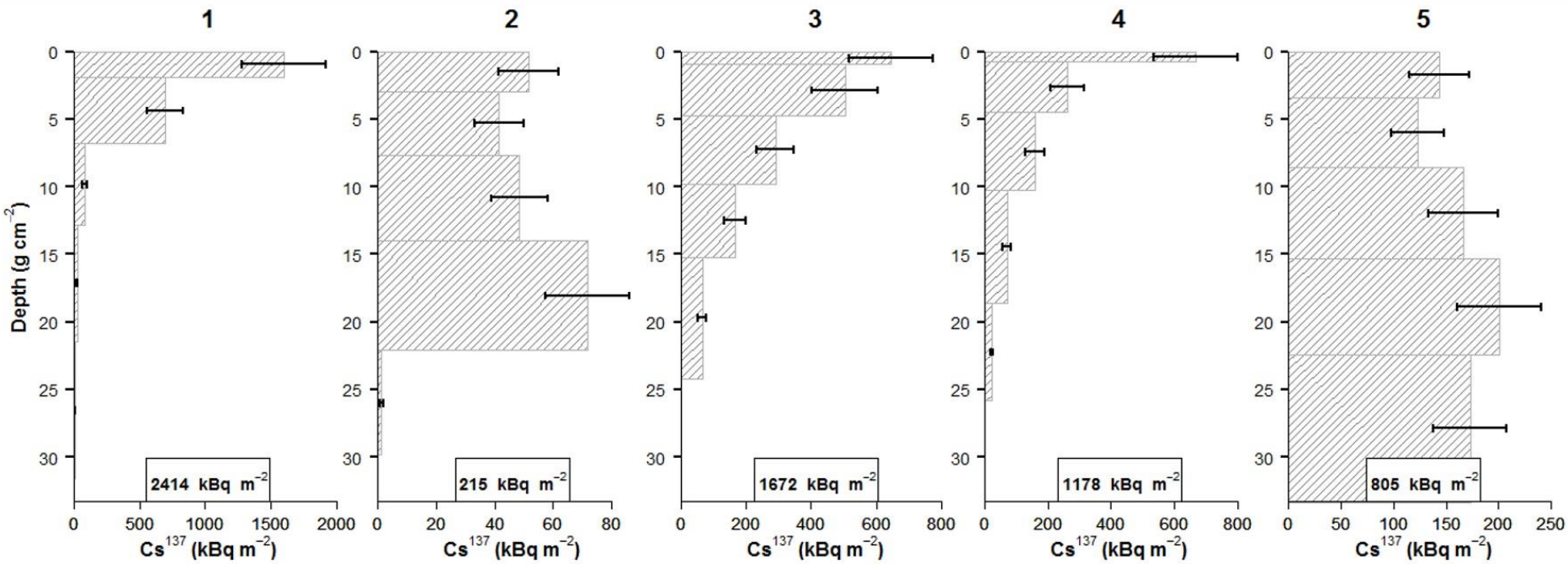

843

844 ***Figure 5***

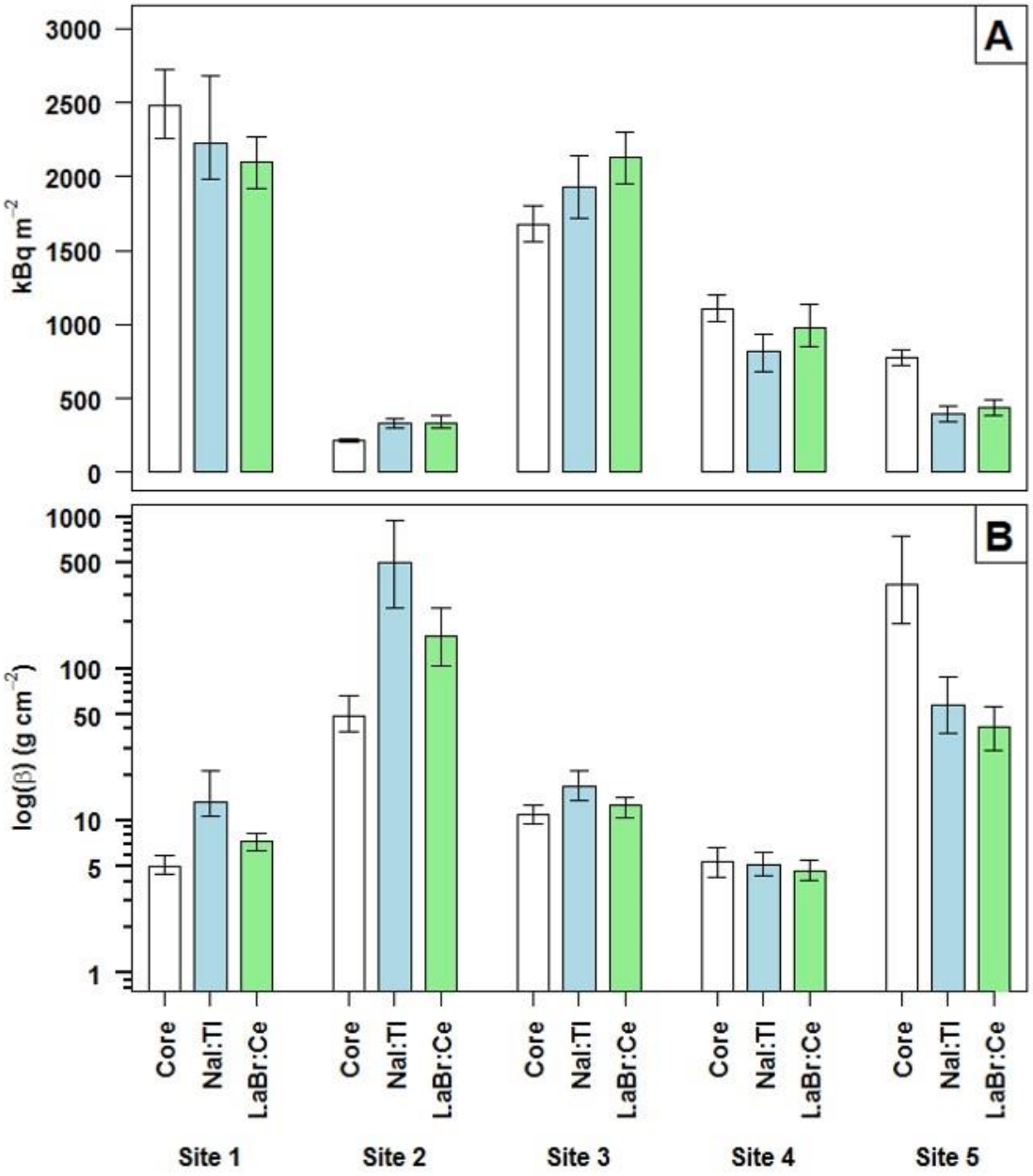
A
B
kBq m^{-2}
log(β) (g cm^{-2})
3000
2500
2000
1500
1000
500
0
1000
500
100
50
10
5
1
Core
NaI:Tl
LaBr:Ce
Site 1
Site 2
Site 3
Site 4
Site 5

Figure 6

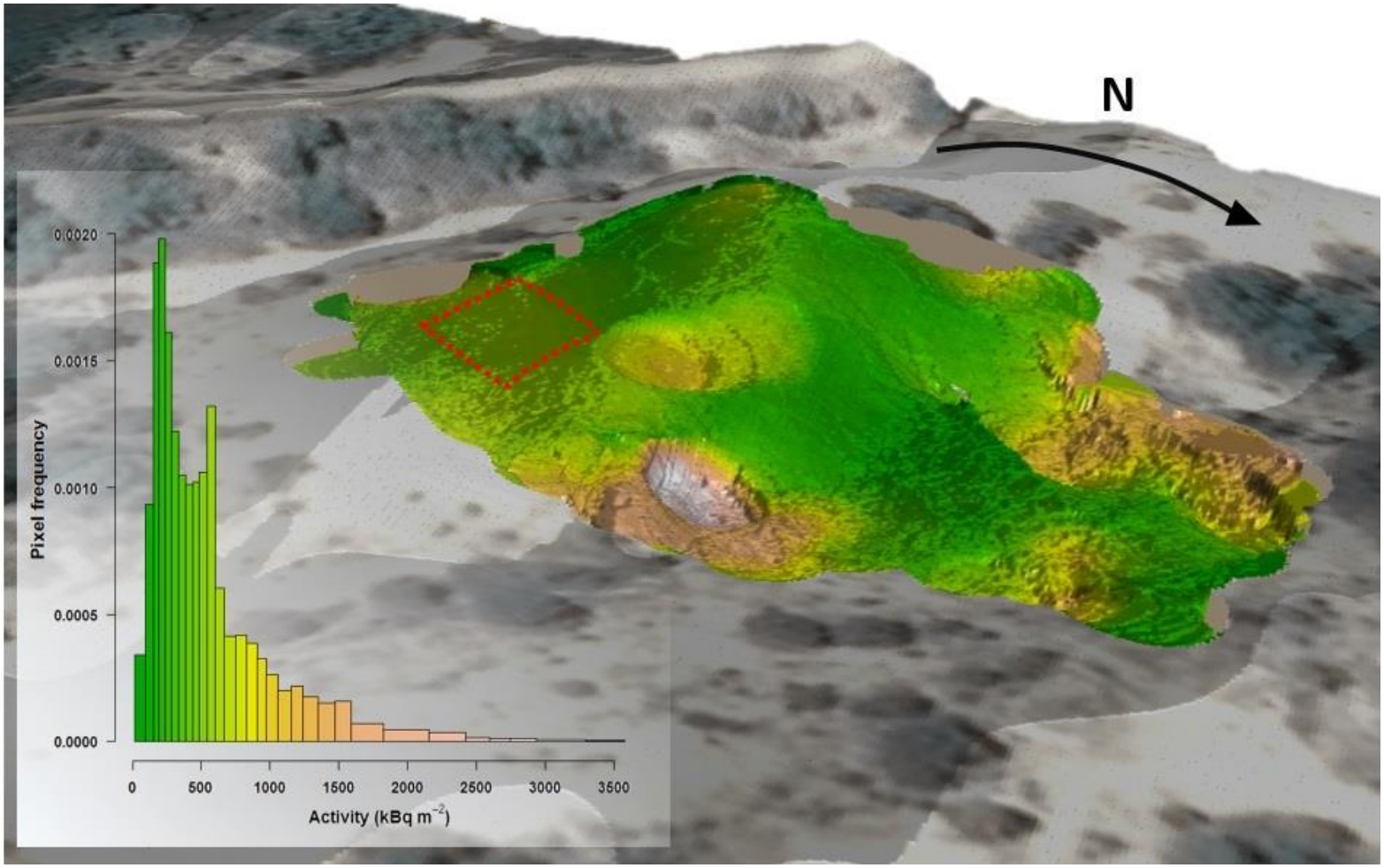

Graphical abstract

853